Ultrasonics - Sonochemistry 68 (2020) 105196

Contents lists available at ScienceDirect

Ultrasonics - Sonochemistry

journal homepage: www.elsevier.com/locate/ultson

Ultrasonic degradation of perfluorooctane sulfonic acid (PFOS) correlated with sonochemical and sonoluminescence characterisation

Richard James Wood[a], Tim Sidnell[a], Ian Ross[b], Jeffrey McDonough[c], Judy Lee[a], Madeleine J. Bussemaker[a,*]

[a] Department of Chemical and Process Engineering, University of Surrey, Guildford, Surrey GU2 7XH, United Kingdom
[b] ARCADIS, Global Remediation, 10th Floor, 3 Piccadilly Place, Manchester, Greater Manchester M1 3BN, United Kingdom
[c] ARCADIS US 630 Plaza Drive Suite 200 Highlands Ranch, CO 80129, United States

A B S T R A C T

Sonolysis has been proposed as a promising treatment technology to remove per- and polyfluoroalkyl substances (PFASs) from contaminated water. The mechanism of degradation is generally accepted to be high temperature pyrolysis at the bubble surface with dependency upon surface reaction site availability. However, the parametric effects of the ultrasonic system on PFAS degradation are poorly understood, making upscale challenging and leading to less than optimal use of ultrasonic energy. Hence, a thorough understanding of these parametric effects could lead to improved efficiency and commercial viability. Here, reactor characterisation was performed at 44, 400, 500, and 1000 kHz using potassium iodide (KI) dosimetry, sonochemiluminescence (SCL), and sonoluminescence (SL) in water and a solution of potassium salt of PFOS (hereafter, K-PFOS). Then the degradation of K-PFOS (10 mg L^{-1} in 200 mL solution) was investigated at these four frequencies. At 44 kHz, no PFOS degradation was observed. At 400, 500, and 1000 kHz the amount of degradation was 96.9, 93.8, and 91.2%, respectively, over four hours and was accompanied by stoichiometric fluoride release, indicating mineralisation of the PFOS molecule. Close correlation of PFOS degradation trends with KI dosimetry and SCL intensity was observed, which suggested degradation occurred under similar conditions to these sonochemical processes. At 1000 kHz, where the overall intensity of collapse was significantly reduced (measured by SL), PFOS degradation was not similarly decreased. Discussion is presented that suggests a hydrated electron degradation mechanism for PFOS may occur in ultrasonic conditions. This mechanism is a novel hypothesis in the field of PFAS sonolysis.

1. Introduction

Perfluorooctanesulfonic acid (PFOS) is one of many per- and polyfluoroalkyl substances (PFASs). It is one compound in a group of variable chain length perfluoroalkyl acids (PFAAs) with a sulphate functional group, which are more broadly referred to as perfluorosulfonic acids (PFSAs). PFSAs have the configuration $C_nF_{2n+1}SO_3H$, PFOS having eight perfluoroalkyl carbon atoms (C8) [1–3]. PFSAs do not fully mineralise in the environment; however, some PFASs can biotransform into perfluoroalkyl acids (PFAAs). This leads to a decrease in chain length which makes the molecules increasingly soluble in water and therefore more mobile in the natural environment [4–7]. The potassium salt of PFOS has a solubility of around 520 mg L^{-1} at 20 °C [8,9] and, as a surfactant, has both hydrophobic (perfluoroalkyl group) and hydrophilic (sulfonate group) components [10]. PFASs are commonly used throughout industry (e.g. in firefighting foams) and are linked to harmful effects in humans and animals [11]. The current practice for aqueous PFAS treatment is to concentrate large volumes of impacted waters to improve the economics of energy-intensive destruction technologies (e.g. incineration) [10,12]. As a result of the costs associated with high temperature incineration of PFASs, there is a need for more effective mineralisation/destruction methods [10,13]. The difficulty in achieving complete mineralisation of PFASs comes from their multiple and extremely strong C–F bonds [14,15]. Additionally, the adjacent fluorine atoms along the perfluroalkyl chain can electrostatically and sterically shield the carbon–carbon bonds from direct attack [16]. A detailed description of PFAS treatment methods and degradation mechanisms can be found in previous reviews [7,10,13,17–18].

This work considers the degradation of K-PFOS via sonolysis. Ultrasonic cavitation has the potential to degrade PFOS, as attributed to high temperature pyrolysis during bubble collapse [19–27]. Moriwaki *et al.* showed a 28% and 60% degradation for 10 mg L^{-1} PFOS solution under air and argon, respectively, at 200 kHz (3 W cm^{-2}) [19]. Other authors observed PFOS degradation of up to 99% of its initial concentration at 358 kHz and suggested that the mechanism was pyrolysis at the high temperature bubble surface [21]. Theoretically, the ionic functional group could be initially cleaved via pyrolytic C-S bond cleavage, followed by mineralization of the perfluoroalkyl group, as indicated by stoichiometric release of sulphate as PFOS degrades [28]. However, other research groups have indicated that defluorination occurs more readily before functional group cleavage [24]. This is

* Corresponding author.
E-mail address: m.bussemaker@surrey.ac.uk (M.J. Bussemaker).

https://doi.org/10.1016/j.ultsonch.2020.105196
Received 16 August 2019; Received in revised form 27 May 2020; Accepted 27 May 2020
Available online 13 June 2020

consistent with the formation of low molecular weight compounds which would suggest that ionic functional group cleavage is not the initial stage of decomposition [19], likely due to the poor leaving ability of the sulfonate functional group. The degradation of 10, 100, and 460 μM concentrations of PFOS, under ultrasound at 25, 500, and 1000 kHz found the highest frequency to be most effective, attributed to an increase in the number of active bubbles in solution [25]. This observation conflicts with other work across similar frequencies which found that 358 kHz was the most effective [21]. The ability for PFOS degradation to occur is proposed to be limited by the available active bubble surface area, which becomes readily saturated with PFOS molecules [22,27].

The hydrophobic, lipophobic, and fluorophillic nature of the perfluoroalkyl moiety in PFOS will cause aggregation (or self-assembly) of PFOS at gas–liquid interfaces [29,30]. PFOS also has a low vapour pressure and thermal stability and is therefore unlikely to readily vaporise inside the bubbles [19]. Ultrasound applied at mid to high frequencies (~300–1000 kHz) can generate significant numbers of radicals due to the transient nature of cavitation and an increase in the number of bubbles [31,32]. Hence, PFOS has a certain stability at the bubble interfacial region (or surface), where it is exposed to radical-mediated reactions [33,34]. Besides radical species, hydrated electrons are debated to exist (with short lifetimes) at the bubble interface and possibly in the bulk solution [35–38], although they have only been detected at high frequency and/or in alkaline solutions [35,38,119]. Therefore, the discussion of the data in this work explores the potential that the PFAS sonolytic reaction mechanism involves the emission of hydrated electrons from a non-equilibrium plasma, a concept which has been discussed in other PFAS degradation techniques [39–42] but not in the context of PFAS sonolysis.

Additionally, there is still little information regarding the effects of frequency, in terms of the standing to travelling wave ratios and bubble characteristics on the degradation of PFOS. Therefore, the ultrasonic reactor in this work is characterised through KI dosimetry, sonochemiluminescence (SCL), and sonoluminescence (SL) to elucidate the yields and spatial distribution of sonochemical activity at different frequencies. The rates of PFOS degradation and release of fluoride ions are then compared to the various characteristics of the ultrasonic field, as determined using these characterisation techniques. Such characterisation and comparison have yet to be completed in literature with respect to PFAS degradation and frequency effects. This yields valuable information on the reaction mechanism under various operating conditions and the enhancement of reaction rates through the determination of optimum bubble conditions.

2. Experimental

2.1. Materials and conditions

98% Heptadecafluorooctanesulfonic acid potassium salt, 99.5% (reagent grade) potassium iodide (KI), analytical standard 0.1 M sodium fluoride and 97% luminol (5-amino-2,3-dihydro-1,4-phthalazinedione) were acquired from Sigma-Aldrich®. Ionic strength adjustor (ISA) TISAB I was purchased from Cole-Parmer. All solutions were made using distilled water (Milli-Q) from an Elix Essential 3 (UV) Type 2 operating at 14.5 MΩ cm.

2.2. Reactor configuration

The amplifier, step up transformer, glass reactor, and cooling jacket circulation system were used as previously reported [43–45] and for convenience these are shown in the Supplementary information (Fig. S1). The transducers were made by Honda Electronics Co. LTD. and are composed of piezo-electric ceramics, 5 cm in diameter, connected to a vibration plate 10 cm in diameter. The contact area of the transducer to the liquid was 6.6 cm in diameter. The frequencies of operation of the four ultrasonic plates were 44, 400, 500, and 1000 kHz, respectively. The height of liquid in the reactor was 58 mm. Experiments were conducted at room temperature (25 ± 3) °C. A cooling jacket with water was employed to ensure the temperature of solution did not increase beyond 45 °C. This was done to control experimental parameters as far as reasonably practicable and to prevent damage to the ultrasonic electronics. Argon saturated solutions have enhanced sonolytic reaction rates, compared to air saturated solutions, due to argon's high polytropic index [46,47]. While this is also true in the case of PFOS degradation [19], all experiments were conducted in an air atmosphere since this is more likely to reflect the gaseous environment used in an industrial clean-up of PFASs, due to the high cost of argon.

2.3. Reactor characterisation

2.3.1. Calorimetry

To calculate the ultrasonic power in solution, the calorimetric power was determined via Equation 1 [48].

$$P = mC_P\frac{dT}{dt} \quad (1)$$

Where;

$m = Mass\ of\ water\,(g)$

$C_P = Specific\ heat\ capacity\ of\ water\ (4.19\ J\ g^{-1}\ K^{-1})$

$\frac{dT}{dt} = Rate\ of\ solution\ temperature\ increase\ during\ sonication\ (K\ s^{-1})$

All calorimetry experiments were repeated a minimum of three times and the average calorimetric powers and standard deviations calculated, shown in Table 1.

2.3.2. KI dosimetry

KI solution (0.1 M) was used to give an approximate measure of overall sonochemical activity via the oxidation of iodide ions to the triiodide ion (I_3^-) in solution, for which a detailed reaction scheme has been presented previously [49]. Detection and quantification of the triiodide ion was completed using UV–Vis spectrophotometry at 355 nm and a molar absorptivity of 26,303 L mol^{-1} cm^{-1}, via Beer's law [48]. As per previous work, the sonication time for KI dosimetry was 14 min [43–45]. However, nitrogen in air saturated systems can be converted into nitrous acid under ultrasound which, in turn, can oxidise KI [49]. Further, this reaction is catalysed by oxygen in the air [50,51]. Ergo, the authors acknowledge the limitations of this method for quantifying hydroxyl radical-mediated production via I_3^- detection for an air saturated system. Hence, KI dosimetry was used as an approximation of the *relative* differences in I_3^- production (and hence overall sonochemical activity) between frequencies. The KI dosimetry results were also used to support the other metrics of sonochemical activity used in this work, i.e. calorimetry, sonoluminescence, and sonochemiluminescence. All KI dosimetry data were measured at least three times with the averages and standard deviations calculated, as shown in Fig. 3c.

Table 1
Calorimetric powers for frequencies 44, 400, 500 and 1000 kHz at 40 W. The RP values represent the reflected power from the transducer to the amplifier due to poor impedance matching. Each frequency was tuned to an applied frequency to minimise reflected power (RP).

Frequency (kHz)	Applied Frequency (kHz)	Reflected Power (RP) (W)	Calorimetric Power (W)
44	44.9	8	20.8 ± 0.9
400	402.6	0	30.5 ± 0.3
500	500.0	0	32.0 ± 0.8
1000	996.1	0	34.6 ± 0.2

2.3.3. Sonochemiluminescence/sonoluminescence image analysis

Image analysis of SCL and SL was used to provide information regarding the intensity and location of active cavitation using a basic (0.1 M NaOH) 1 mM luminol solution (SCL) [52], Milli-Q water (SL) [49] and 18.5 μM (10 mg L^{-1}) K-PFOS solutions (SL). SCL imagery was used to evaluate the spatial distribution of chemical activity using the reaction of luminol with the superoxide radical anion in solution [53]. SL imagery captures luminescence from inside the collapsing bubbles due to molecular disassociation/ionisation. Spatial distribution and light quantification of both SCL and SL was performed with an ANDOR iXon3 EMCCD camera and software. The camera was operated at −70 °C with an EM gain level / exposure time (seconds) of 50 / 20 for SL and 4 / 4 for SCL. The decrease in gain / exposure time for SCL was to protect the camera from exceeding its recommended intensity limits. Light intensity measurements were used for quantitative analysis, then for qualitative analysis, the imagery was optimised by changing the limits of the software filter, hence the differing background brightness for different frequencies, displayed in Fig. 4. All SL and SCL data were measured at least three times with the averages and standard deviations calculated as shown in Fig. 3.

2.3.4. Calculation of rate constants

Two sets of data were available for calculation of rate constants: 1) The concentration of PFOS with time and 2) Fluoride release with time. However, it was noted that the reaction order appeared to change with time, ergo an initial zero order reaction rate was calculated for the first two hours of the reaction and a first order reaction rate calculated for the latter two hours. First, the data were plotted on both linear–linear and log-linear plots with a linear trendline and the R^2 values assessed to determine the rate order. All graphs plotted to determine rate order are included in Supplementary information, Figs. S2–S4. Then, the slope of the relevant plot was taken as the rate constant, using Eqs. (2)–(4).

$$r_X{}^{0th} = k_X{}^{0th} = \frac{\Delta C_X}{\Delta t} = \frac{C_{X,t=120mins} - C_{X,t=0mins}}{120minutes} \quad (2)$$

$$r_X{}^{1st} = k_X{}^{1st} C_{X,t} \quad (3)$$

$$k_X{}^{1st} = \frac{\ln(C_{X,t=240mins}) - \ln(C_{X,t=120mins})}{120minutes} \quad (4)$$

where;

$X = PFOS \text{ or } F^-$

$r_X{}^{0th} = Zeroth\ order\ reaction\ rate\ for\ component\ X$

$k_X{}^{0th} = Zeroth\ order\ rate\ constant\ for\ component\ X$

$\frac{\Delta C_X}{\Delta t} = Change\ in\ concentration\ of\ species\ X\ with\ time$

$C_{X,t} = Concentration\ of\ X\ at\ a\ time\ (t)$

$r_X{}^{1st} = First\ order\ reaction\ rate\ for\ component\ X$

$k_X{}^{1st} = First\ order\ rate\ constant\ for\ component\ X$

Note that, for the fluoride release, calculation of a first order rate constant between times 0 and 120 min is not feasible since the fluoride concentration at time t = 0 min is 0 and a natural log of $C_{F^-,0}$ cannot be taken. All rate constants are calculated based on the average data from at least three experimental repeats and standard deviations given in Table 3.

2.4. K-PFOS degradation analysis and experimentation

2.4.1. K-PFOS Sonication procedure

Aside from the glass reactor, polypropylene containers and pipettes were used at all times since PFOS can be irreversibly adsorbed to glass [54]. K-PFOS solution (~100 mg L^{-1}) was diluted to 10 mg L^{-1} (18.5 μM) for use as stock solution. The volume of sonicated stock solution was 200 mL and the applied power for all frequencies was 40 W. The applied sonication time was 4 h and 2 mL samples were taken every hour (starting from 1 h) for fluoride analysis, and 5 mL for PFOS analysis in the additional set of experiments (see Section 2.4.2). To protect the transducers from heat damage, sonication was performed in 20-minute intervals with 5-minute cooling periods between each progressive sonication. Thus, the total time the K-PFOS solution was in the reactor was 295 min. The solution weight was recorded before and after the 4-hour sonication period and a lid was fitted to the vessel during sonication to minimise losses due to ultrasonically-induced mist formation and possible evaporation of water and volatile compounds. The average loss of solution after 4 h sonication, when PFOS and fluoride analysis was performed, was 26.4 ± 0.7 g, (for all frequencies), including loss due to sampling (~21 g). The average maximum temperature reached during sonication was 42.8 ± 2.1 °C. All sonication experiments were repeated a minimum of three times and the data averages and standard deviations calculated, as shown in Fig. S5.

2.4.2. Perfluorinated compound and fluoride analysis

Initially, analysis of fluoride release from sonication of 10.0 mg L^{-1} of K-PFOS was completed using a Cole-Parmer Combination Fluoride Ion Selective Electrode, for a minimum of three repeats. For all conductivity readings, a volume of ISA equal to 10% of the sample was added to the solution, the electrode inserted, and the solution mixed at 100 rpm using a magnetic stirrer. Once the conductivity reading stabilised to within ± 0.05 mV, the temperature was gently increased to 25 °C ± 0.05 °C using a hot plate and the conductivity recorded. The electrode was calibrated with a dilution series made using a 0.1 M standard of NaF diluted from 0.1 to 10^{-5} M, each one decade apart. The calibration data was produced in triplicate and a correlation derived between the fluoride ion concentration and conductivity is summarised in Eq. (5).

$$[F^-] = 0.0073e^{-0.039\sigma} \quad (5)$$

Where;

$[F^-] = Concentration\ of\ fluoride\ ions\ (\text{mol } L^{-1})$

$e = Exponential\ number$

$\sigma = Conductivity\ (mV)$

To analyse reaction progression, 2 mL samples were taken from the reactor and analysed once per hour. The fluoride concentration at time zero was subtracted from all subsequent readings to account for F^- ions present in the Milli-Q water. Further, 200 mL of Milli-Q water was sonicated without the presence of K-PFOS to measure the conductivity due to the possible breakdown of fluorine containing species in the water. The values recorded at each hour for the sonication of water were subtracted from the PFOS sonication readings. The average fluoride reading for the initial K-PFOS solution was 9.03 μM and sonication of Milli-Q water produced 2.73 μM (equivalent to 2.9 mol% and 0.86 mol%, respectively, of fluorine contained in the initial K-PFOS).

Additional samples of the sonicated K-PFOS solutions were sent to ALS Environmental (UK) for PFAS analysis using LC-MS/MS [55], and fluoride and sulphate analysis using spectrophotometry [56,57]. Sonication of 9.42 mg L^{-1} (17.5 μM) PFOS solution was performed under identical conditions to the samples used for fluoride probe analysis. Then analysis was performed to identify perfluorinated compounds (C4–C12). The full suite of target analytes and detection limits are provided in the Supplementary information (Table S1). PFASs were analysed from a 1 in 10 dilution of 5 mL samples and complementary fluoride analysis was performed using direct samples of 2 mL every hour. The vessel and transfer beakers were rinsed with methanol, and the methanol wash was sent for analysis with the sonicated samples. pH

Table 2
Fluoride release and PFOS degradation after four hours for frequencies 44, 400, 500 and 1000 kHz at 40 W, using the different analytical techniques.

Frequency (kHz)	Fluoride release after 4 h, as measured by:				PFOS degradation after 4 h, (ALS LC-MS/MS)
	F^- probe		ALS Spectrophotometry		
	%	μM	%	μM	%
44	0.0 ± 3.4	0.0 ± 10.7	0.0 ± 0.0	0.0 ± 0.0	0.0 ± 0.0
400	99.5 ± 4.9	314.3 ± 15.5	95.0 ± 13.2	300.0 ± 42.1	96.9 ± 3.0
500	100.0 ± 2.8	315.9 ± 8.8	92.8 ± 15.5	293.2 ± 48.9	93.8 ± 3.0
1000	100.0 ± 8.2	315.9 ± 25.9	95.0 ± 13.2	300.0 ± 42.1	91.2 ± 2.7

change was also measured using both a Hanna HI 8424 and a Mettler Toledo 5GO F2 pH meters. The pH of the initial solution and final reaction products were measured at 21.3 °C. Each measurement was repeated a minimum of three time so that the average change in pH and standard deviation could be plotted for all four frequencies.

3. Results and discussion

3.1. K-PFOS degradation by sonolysis

The results of the fluoride analysis using the fluoride probe and ALS spectrophotometry after 4 h of sonication, are shown in Table 2. Note that the theoretical yield of fluoride ions given 100% PFOS degradation is 315.9 μM (6.001 mg L^{-1}) from the initial 10 mg L^{-1} K-PFOS. Excluding the 44 kHz results, the two fluoride analysis methods have an average agreement within ± 7%, with a maximum discrepancy of ± 15%. When accounting for the slight difference in initial K-PFOS concentrations between methods (10 mg L^{-1} vs 9.42 mg L^{-1}) the average agreement is ± 1% with a maximum discrepancy of 14%. PFOS sorption onto the glassware was not accounted for in the fluoride electrode analysis and does not appear to significantly affect the results when compared with the ALS analysis.

Plots of fluoride release as measured by the fluoride probe and ALS spectrophotometry are shown in Figs. 1 and 2, respectively. Both fluoride analyses suggest that mineralisation is completed within 3 h of sonication at 400 and 500 kHz, but at 1000 kHz fluoride continues to be released after 3 h. The experimental error associated with the probe is approximately 3.4%, since the 44 kHz sonication showed ±3.4% degradation, and the 500 kHz sonication showed 103.3% degradation at 3 h and a return to 100% release at 4 h (Fig. 1). Assuming complete degradation of the PFOS molecule, this error corresponds to ± 340.0 μg L^{-1} (0.632 μM) PFOS, 3.1% of the initial solution concentration. It is difficult to see the variation in degradation rates between different frequencies at low PFOS concentrations (i.e., nearing 3 h sonication) but fluoride release in the first 2 h differs more significantly between frequencies. By considering Figs. 1 and 2, 400 kHz shows the greatest initial (within the first 2 h) fluoride release, followed by 500 kHz, then 1000 kHz.

The degradation of PFOS in solution after 4 h, analysed by ALS, is shown in Table 2. The variation of measured PFOS degradation values at 44 kHz is within experimental error (± 282.4 μg L^{-1} {0.565 μM}) showing that the sonication at this frequency is ineffective. This error represents 3.0% of the initial PFOS concentration. All frequencies showed an increase of ~20 °C in bulk temperature during sonication (see Fig. S5) and the applied frequencies induced mechanical agitation of the solution, as expected [58,59]. The lack of PFOS degradation at 44 kHz suggests that the increase in bulk temperature and liquid agitation due to the applied ultrasound do not influence PFOS degradation. Previous reports on low frequency (20 kHz) degradation of PFOS are limited to trace levels (pM), using an ultrasonic horn [61]. Degradation rates at higher frequencies are of the same order of magnitude as previous work (reported rate constant of 2.8×10^{-2} min^{-1} at 358 kHz in argon at 10 °C [22]), as shown in Table 3. The fluoride release as measured by the electrode analysis and ALS spectrophotometer shows zero order kinetics in the initial 2 h of sonication (Table 3). The fluoride measurements via electrode analysis and those given by ALS have similar values. Within the first 2 h, both analyses show that 400 kHz has the least agreement with zero order kinetics and 1000 kHz has the best agreement (Figs. 1 and 2). Beyond the 2 h mark, all frequencies showed pseudo first order kinetics, with the switch between the two reaction orders occurring somewhere between 2.3 and 2.9 μM PFOS, as is consistent with previous literature [20,22,27].

Both the stoichiometric release of fluoride ions at 400, 500, and 1000 kHz (Fig. 2) and the complete degradation (at 400 and 500 kHz) indicate that sonolysis under these conditions completely degraded PFOS without significant formation of less fluorinated shorter chain

Table 3
Fluoride release and PFOS rate constants within the initial and final two hours for frequencies 44, 400, 500 and 1000 kHz at 40 W, using the different analytical techniques.

Frequency (kHz)	Zero order fluoride release rate constant (μg L^{-1} min^{-1}) within 0–2 h, as measured by:				Zero order PFOS rate constant within 0–2 h (μg L^{-1} min^{-1}), as measured by:	
	F^- probe	(R^2)	ALS Spectrophotometry	(R^2)	ALS HPLC/MS	(R^2)
44	N/A	N/A	N/A	N/A	N/A	N/A
400	42.7 ± 1.8	(0.9659)	40.1 ± 4.4	(0.9481)	−66.5 ± 7.3	(0.9298)
500	39.8 ± 3.0	(0.9912)	36.8 ± 4.1	(0.9892)	−54.2 ± 6.0	(0.9448)
1000	38.5 ± 3.1	(0.9999)	32.9 ± 3.6	(0.9826)	−53.1 ± 5.8	(0.9710)
Frequency (kHz)	**First order fluoride release rate constant ($\times 10^{-3}$ min^{-1}) within 2–4 h, as measured by:**				**First order PFOS rate constant within 2–4 h ($\times 10^{-2}$ min^{-1}), as measured by:**	
	F^- probe	(R^2)	**ALS Spectrophotometry**	(R^2)	**ALS HPLC/MS**	(R^2)
44	N/A	N/A	N/A	N/A	N/A	N/A
400	1.3 ± 0.8	(0.7023)	1.4 ± 0.9	(0.7966)	−1.3 ± 0.04	(0.9056)
500	1.9 ± 0.8	(0.6634)	1.9 ± 0.4	(0.8314)	−1.3 ± 0.04	(0.9966)
1,000	2.2 ± 1.2	(0.8954)	3.1 ± 0.4	(0.9997)	−1.0 ± 0.03	(0.9995)

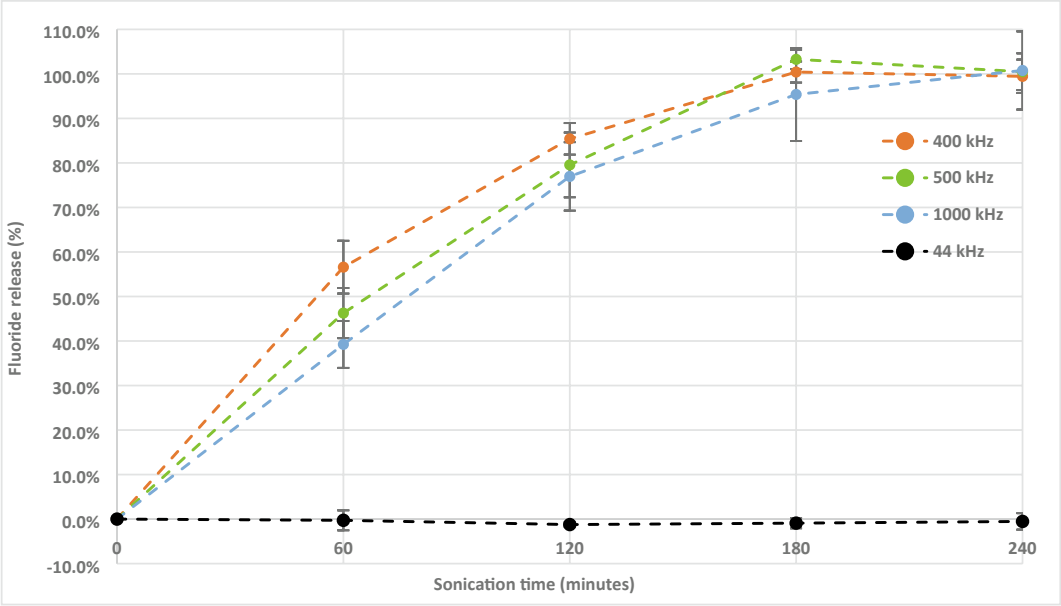

Fig. 1. Percentage fluoride ion release, as measured by the fluoride probe, with time for 44 (black), 400 (orange), 500 (green) and 1000 kHz (blue) at 40 W. Data is given as the average of three replica experiments, with a measured experimental error of ± 3.4%.

PFAAs. Although trace concentrations of some shorter chain PFAAs were detected at all frequencies, the total amount of all short chain species represented less than 1% of the total yield by mass (Table S2). The most significant product was PFOA, which decreased with time, followed by perfluoroheptanoic acid (PFHpA) and perfluorohexanoic acid (PFHxA) that indicates the conversion of PFOS to PFOA and subsequent chain reduction in ultrasonic conditions. The conversion of PFOS to PFOA and subsequent shorter chain formation was previously observed at 200 kHz [19]. PFOS chain shortening was also reported at 500 and 1000 kHz based on comparative sulphate and fluoride release rates rather than specific molecule detection [24,25]. Conversely, authors report that at 354 and 618 kHz the sulphate release was stoichiometric with PFOS degradation [28]. Further, at 575 kHz, PFOS and PFOA were sonicated together and formation of small chain PFCAs and PFSAs was not observed [27]. Hence differing theories around the mechanisms of degradation are proposed, with either initiation via C-S cleavage [28] or by generation of a sono-intermediate species [27]. At the same time, sonolysis degrades shorter chain PFAAs [21,24] hence secondary reactions could proceed too quickly for appreciable degradation products to be realised, as recognised in the sono-intermediate model [27].

The most efficient frequency for PFOS degradation was 400 kHz, followed by 500 kHz and 1000 kHz. Note that the difference between degradation rate constants at 500 kHz and 1000 kHz was not statistically significant. Previous comparisons of frequency settings using 10 μM PFOS found that at 1000 kHz, fluoride release was approximately 1.3-times faster than at 500 kHz [25]. However, the reactor geometry varied between frequencies, making a direct comparison difficult as this will impact the bubble dynamics [47]. Further, the sonication was performed indirectly via submersion of the reaction vessel

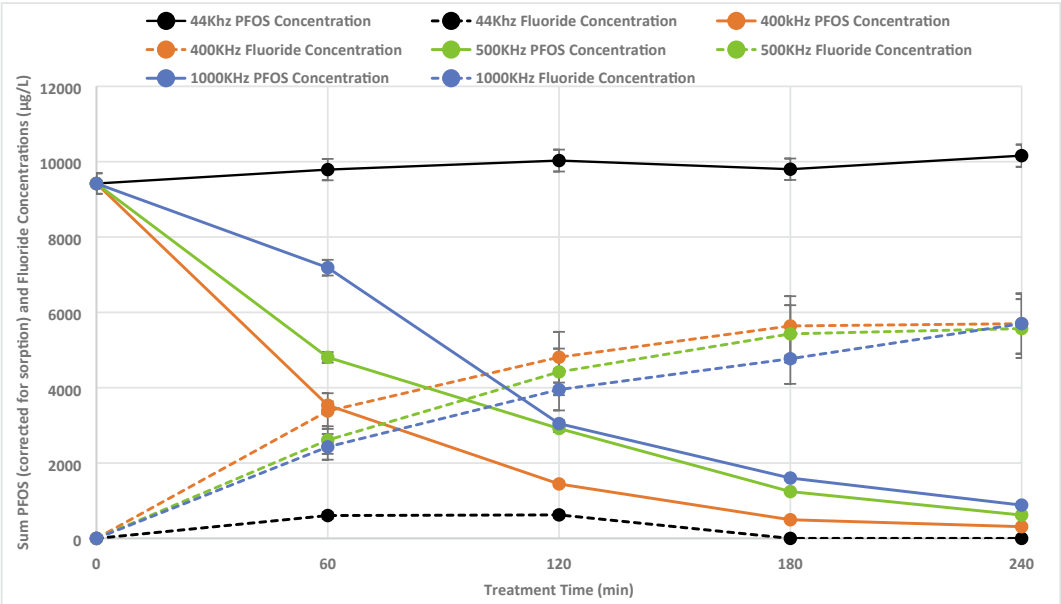

Fig. 2. The reduction in PFOS (solid lines) in 200 mL solutions and associated increase in fluoride (dashed lines) for 44 (black), 400 (orange), 500 (green) and 1000 kHz (blue) at 40 W. Data has a measured experimental error of ± 2.9% for PFOS degradation and ± 14.0% for fluoride release.

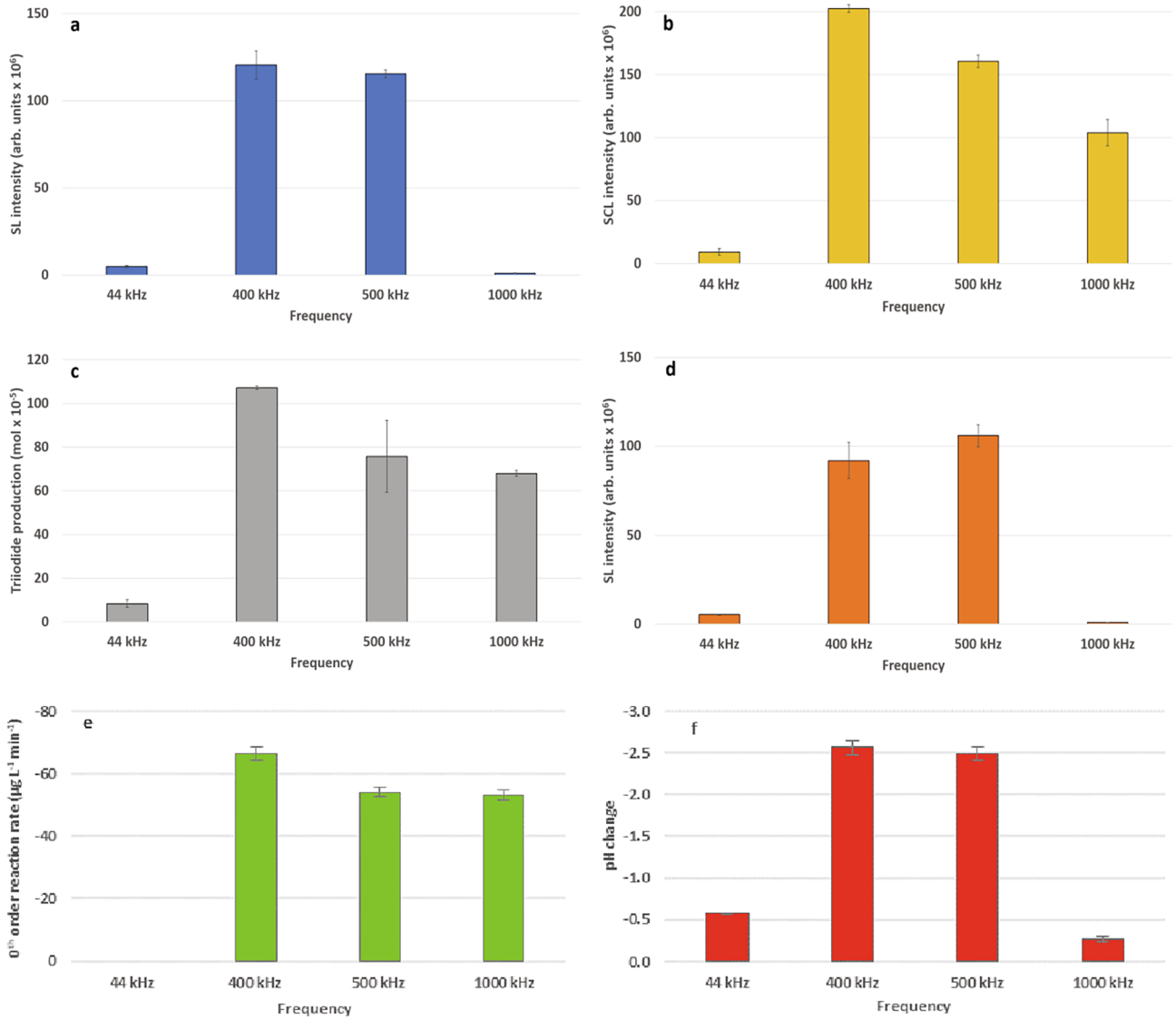

Fig. 3. Graphs of (a) SL intensity from water, (b) SCL from luminol solutions, (c) triiodide production from KI solution, (d) SL intensity from PFOS solution (200 mL solutions), (e) PFOS reaction rate during initial 120 min of sonolysis and (f) pH changes during four hours of sonication from initial pH 5.66 (200 mL solutions).

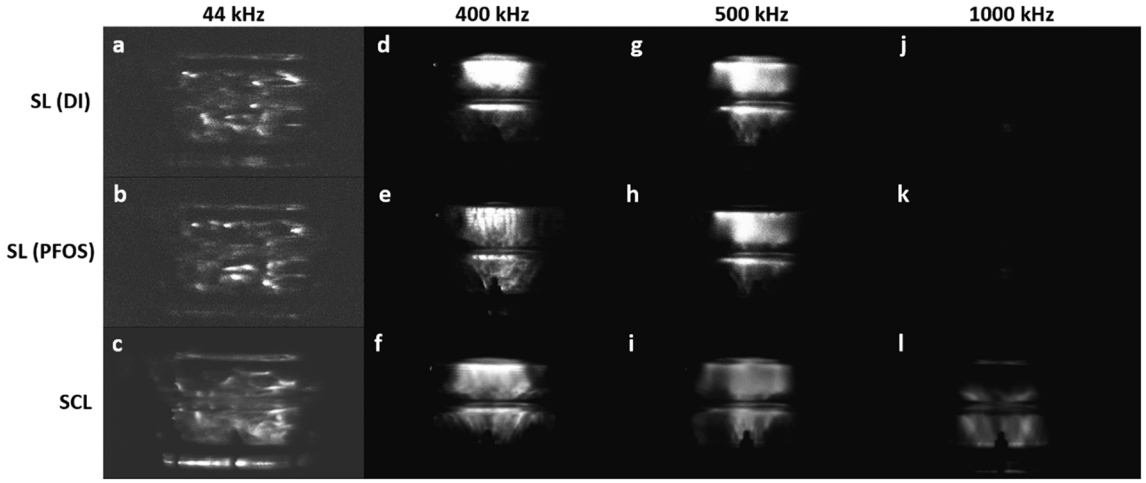

Fig. 4. SL active bubble distributions from water (top) and PFOS (middle), and SCL active distributions from luminol (bottom) for 200 mL solutions at 40 W. The changes in background colour for different frequencies are due to the different limits used by the image software to optimise the light present. The exposure and gain times were the same for each frequency.

in sonicated DI water, as opposed to direct sonication of the PFOS solution in the case of this work. Using a lower initial concentration (in the range of 0.4 μM), degradation of a PFOA / PFOS mixture was fastest at 358 kHz compared to 610 and 202 kHz and the magnitude of the difference increased with power density [20].

There was a difference of around 20 °C between the initial solution temperature and the stable temperature during sonolysis, as well as a difference of around 7.0 °C during sonolysis at the four different frequencies (see Fig. S5). However, these temperature variations do not play a significant role in PFAS degradation since the solution at 44 kHz was heated to around 35 °C and showed no degradation. Furthermore, the thermal decomposition rate of PFOS has been shown to be insignificant below temperatures of around 600 K, with half-lives of several thousand hours even at these elevated temperatures [62]. In other ultrasonic work which degraded PFOA using 40 kHz ultrasound and sulfate ions, the effect of increasing temperature from 25 to 45 °C (similar to the temperature variation in this work) was shown to be minimal compared to the impact of ultrasound and of the sulfate ions [56]. Both the aforementioned paper and a similar work showed that increasing temperatures above 20 °C had a negative effect on PFOA degradation rate [61,63]. This is in opposition to this work, in which increased degradation rates correlated with increased temperature and suggests bulk temperature is a secondary effect of sonication. Finally, multiple works have investigated purely heating of several PFASs (including PFOS) to 40–85 °C noted no degradation (only sorption to glassware) without the use of additional oxidants [64,65]. For these reasons, it appears that such small fluctuations in temperature would not have a significant impact on reaction rate compared to the temperatures achieved within a collapsing bubble, which are in excess of several hundred Kelvin [66].

pH was also altered during the reaction from an initial value of 5.66 to 5.08, 3.09, 3.16, and 5.39 for frequencies of 44, 400, 500, and 1000 kHz, respectively, as shown in Fig. 3f. The relative changes in pH at the different frequencies do no follow the relative changes in PFOS concentration with time, thereby indicating that (at the given pHs) pH is not a dominant factor in PFOS degradation for this experimental arrangement, as was the case in several other works [63,67–68]. This also suggests that pH is not entirely controlled by PFOS breakdown products since, if this were true, one would expect similar changes in pH at 1000 kHz as at 400 and 500 kHz, due to their similar changes in PFOS concentration with time. pH change is therefore likely dominated by breakdown of N_2 in the air saturated solution to form nitric/nitrous acid, which has been shown to be frequency dependant [50].

These various results demonstrate that the rate of degradation of PFOS is frequency dependent. However, it also depends on the characteristics of the reactor. Hence, in the subsequent sections we aim to investigate the bubble characteristics compared to PFOS degradation to further elucidate the observed phenomena.

3.2. Correlation of PFOS degradation with bubble characteristics

The system was characterised at different frequencies (Figs. 3 and 4) using (i) SL intensity and distribution in water, (ii) SCL intensity and distribution in luminol, (iii) triiodide production in potassium iodide solution, and (iv) SL intensity and distribution in PFOS solution. For all characterisation techniques, 44 kHz has a low magnitude of quantified activity (Fig. 3). At 44 kHz, bubbles are expected to be larger in size and fewer in number [60]), the former contributing to increased coalescence to an inactive size [69]. Further, the collapse at this frequency can be more transient [70], which can lead to lower collapse intensity. In this case, we define collapse intensity in terms of internal temperatures reached [71,72]. These factors contribute to the lower total integrated intensities of SCL and SL, and reduced triiodide production compared to other frequencies, as observed. The reduced activity (SCL and SL) at 44 kHz is congruent with no significant observation of PFOS degradation at this frequency. Reports of PFOS degradation at low frequency are limited to trace amounts (< 0.002 μM) [61]; however, PFOA has been degraded at lower frequencies combined with oxidants such as carbonate [73], sulphate [63], and periodate [68], with various radical-mediated processes proposed. However, PFOS is not effectively degraded by radical-mediated mechanisms nor oxidative processes alone [4,10,13], so the bubble collapse mechanisms at 44 kHz, which are more transient, less spherical [74], and provide a lower surface area to volume ratio [75], are not suited to PFOS degradation at higher concentrations.

In the low-mid frequency range, standing wave formation throughout the solution is expected to dominate [43]. This is observed here at 44 and 400 kHz, where lines of activity are observed within the reactor for SL and SCL (Fig. 4a – f). At 400 and 500 kHz, there is reflection of the sound field at the surface of the solution and enhanced standing wave formation (Fig. 4d – i). However, at 1000 kHz, where the bubbles are smaller in size but greater in number [60], no appreciable SL is observed. This is due to reduced standing wave proportions at higher frequency [76] and weaker individual bubble collapse intensity [70,72,77]. Higher frequencies are often characterised with an area of standing wave activity toward the surface of the solution, as observed in previous work in the same reactor with 400 mL solution [43]. However, the reduced height at 200 mL reduces attenuation of the sound field, preventing standing wave formation at the surface [78]. All frequencies will have some combination of standing and travelling waves as can be seen with the formations at both 400 and 500 kHz (Fig. 4d – i).

The relative changes in SL between frequencies (Fig. 4e, h, and k) indicate that there is a reduction in overall collapse intensity for the 1000 kHz system, as previously observed at higher frequencies [79]. Here, at this higher frequency, bubbles will be smaller in size than the lower frequency systems [60]. However, both the sonochemical processes, SCL and iodide oxidation, and PFOS degradation still show significant activity. The standing wave formation at 400 kHz likely promotes the sonochemical processes and the sonochemical activity tends to decrease in the order of 400 > 500 > 1000 kHz similar to the observed PFOS degradation. Specifically, the total iodine-complex production at 400 kHz is ~ 1.6-times and ~ 1.4-times production at 1000 and 500 kHz, respectively. Then, SCL intensity at 400 kHz is ~ 2.0-times and ~ 1.3-times that at 1000 kHz and 500 kHz, respectively. PFOS degradation within the initial two hours at 400 kHz is in a similar range that is ~ 1.2-times as fast as 500 and 1000 kHz. The SL does not follow any similar correlation when compared to PFOS degradation as SL intensity has similar values at 400 and 500 kHz, and a ~ 100-fold increase in intensity at 400 kHz compared to 1000 kHz. A similar trend is shown when considering pH change (Fig. 3f) and converting to H^+ concentration. Both 400 kHz and 500 kHz reached H^+ concentrations of ~ $10^{-3.2}$ M after four hours of sonication, while 1000 kHz reached $10^{-5.3}$ M, approximately 100 times less concentrated than at 400 kHz and 500 kHz. Hence, the relative shape of Fig. 3f closely resemble those of Fig. 3a and d. This suggest that pH changes in ultrasonic systems are also dependant on bubble conditions which favour SL.

The association of PFOS degradation with conditions that promote sonochemical processes was previously observed when 1000 kHz degraded PFOS 1.3-fold faster than 500 kHz [25]. The hydroxyl radical production under these conditions was 4.1-times higher at 1000 kHz compared to 500 kHz. There is no consistent and direct correlation between the sonochemical processes and PFOS degradation in consideration of the past and present work. However, PFOS clearly does not require the same high intensity collapse conditions (evidenced by SL), but rather is maximised when sonochemical processes are also maximised.

The SL images (Fig. 4a and b) show that at 44 kHz there is little change in the active SL bubble distributions between PFOS and water, hence the similar levels of SL intensity (Fig. 3a and d). At 400 kHz, SL intensity from PFOS is reduced by 23.5% in comparison to water (Fig. 3a and d). The images show reduction in the standing wave at the

surface for the PFOS solution, along with more distributed activity throughout, with some vertical streaming lines (Fig. 4d and e). At 500 kHz, the two SL active distributions for water and PFOS solution are similar (Fig. 4g and h), although SL intensity shows a small but significant 8% decrease for PFOS solution (Fig. 3a and d). At 1000 kHz, SL was detected in very small amounts (Fig. 3a and d). Therefore, conditions that favoured PFOS degradation (400 kHz) also demonstrated a reduction in SL in PFOS solutions compared to water.

This reduction in SL, congruent with favourable PFOS degradation, may indicate quenching of SL by evaporation of PFOS into the bubble as observed with other organics [80]. However, this is unlikely due to PFOS's low volatility [19], as also suggested for other surfactants [81]. Coalescence can be reduced in the presence of surface-active solutes [82] reducing the mean bubble radius, as observed for sodium dodecylsulphate (SDS), which can reduce growth to active SL size [83]. Provided a reduction in coalescence does not inhibit bubble growth to the rectified diffusion [84] or Blake threshold, [69] other effects can take place. Surfactants can increase bubble transience [85] which, in turn, may reduce the intensity of collapse [86] or increase bubble fragmentation, reducing the number of SL emission cycles [71]. Also, rectified diffusion may be increased [85], reducing collapse intensity as more polyatomic gas enters the bubbles [87]. Hence PFOS will likely cause reduced bubble size and/or reduced collapse intensity when added to water.

The SL images of water and PFOS solution at 400 kHz (Fig. 4d and e) show a reduction in the travelling wave for PFOS, causing a decrease in SL at the surface of solution, with a more widespread region of activity. This could be due to reduced attenuation of the wave from smaller bubbles (due to reduced coalescence in the presence of PFOS, hence overall a smaller bubble population) and therefore an overall increased stable bubble population. Also, a reduction in SL cycles and increased cavitation events through fragmentation (increased in the presence of a surfactant through increased transience) may provide more surface area for PFOS to adsorb. Since adsorption on the bubble surface is favoured with increased bubble stability [88], most likely the reduction in bubble size through reduced coalescence is favourable to the adsorption of PFOS on the bubble surface and subsequent degradation.

The variation of PFOS degradation shows a balance between collapse intensity and available surface area. At 400 kHz, with the highest degradation, we expect the lowest available surface area (in comparison to 500 and 1000 kHz) but increased collapse intensity. However, at 1000 kHz when we expect a large increase in surface area but reduced collapse intensity, PFOS degradation is still able to take place of the same order. This is likely because smaller bubbles can adsorb more PFOS at their surface, due to their greater stability and a higher surface-to-volume ratio, allowing for more sonochemical reactions to take place [75]. This is supported by no observation of PFOS degradation for the 44 kHz system where, although there is an intense collapse, as measured by SL, no degradation is observed.

3.3. Implications for the PFOS degradation mechanisms by ultrasound

PFOS sonolysis products depend largely on the experimental conditions. Some report complete mineralisation [28] or very low yields of degradation products [19], while others report evidence of incomplete mineralisation [24,25]. This may indicate more than one degradation mechanism which is influenced by the applied ultrasonic parameters. Classical sonochemistry that occurs either via degradation inside the bubble or at the interface via interactions with oxidising radicals does not apply here. Nano-droplet injection would be expected at 44 kHz, where the most transient conditions occur [89], yet no appreciable degradation was observed, supporting the surfactant's resistance to enter the bubbles via these mechanisms. Then, the bubble surface where PFOS resides is the primary site of hydroxyl radical population and recombination [33,34]. The 44 kHz surface availability is reduced due to a reduction in the number of bubbles in comparison to higher frequencies [70]. Further, several studies have shown that oxidation alone of PFOS has yet to be demonstrated [4,10,13].

The general consensus is that PFOS degradation occurs via pyrolysis at the bubble surface [19,28], with the rate limiting step being diffusion to reaction sites [22,27,28]. However, different initiating steps have been proposed; the pyrolytic cleavage of the ionic headgroup [28] or via formation of a sono-intermediate [27]. Both rely on thermal degradation. Thermal degradation of fluorotelomers (a type of PFAS) at 600 °C (~873 K) resulted in by-product formation [90] that was not apparent above 750 °C (1023 K). Then, complete mineralisation is reported to require temperatures in the order of 1000–1200 °C for 2 s (1273–1473 K) [91–93]. Temperatures at the bubble surface for a single bubble have been estimated to be ~1900 K [94], which is well within the required temperature for pyrolysis of the organic compound. However, estimates for the average temperature at the bubble surface in a multi-bubble system place it in the region of ~800 K [66] which follows from nonequilibrium plasma formation where there are a range of temperatures [95]. Frequency and power also determine the temperature upon collapse. A high frequency system (1056 kHz) generally shows reduced bubble temperatures at low powers in comparison to lower frequencies, and only at higher powers can the maximum temperature be equal or greater [31]. Similar data has been presented by other authors [79]. Since the plasma inside a cavitation bubble is known to be very opaque in nature [96], it is likely that a similar temperature trend would be observed at the bubble surface. However, the temperature at the bubble surface is likely close to the water temperature and only greater than water for a brief moment (in the order of nano-milli seconds compared to 2 s treatment time for incineration [91–93]) due to exposure of liquid to the core as bubbles fragment [97]. This effect would be reduced for a higher frequency system where bubble surface instabilities are reduced compared to lower frequencies [70]. Hence in multi-bubble systems, such as those used for PFOS degradation, the surface temperatures may not be large or sustained enough for pyrolytic cleavage. Especially at higher frequencies where collapse temperatures (and bubble transience) can be significantly reduced.

Alternative mechanisms for sonolytic degradation of PFOS may be via plasma-induced degradation mechanisms. Nonequilibrium plasmas have been evidenced in multi-bubble systems in aqueous solutions and are not necessarily accompanied by SL [95]. Also seen here at 1000 kHz, significant SL conditions are not required for PFOS degradation. Nonequilibrium (or nonthermal) plasmas are characterised by high temperature electrons, hence electron activity at the bubble surface and potentially some ejection into bulk solution is likely to occur, alongside higher detection of sonochemical activity. Hydrated electrons have been suggested as a mechanism for PFAS degradation in plasmas [39], photochemical systems [40,41], and electrochemical treatment [42]. Hydrated electron degradation of PFSAs are proposed to occur via hydrogen/fluorine (H/F) exchange in the middle of the alkyl chain or cleavage of the headgroup [15]. H/F exchange would lead to shorter chain PFSAs and PFCAs, of which only PFCAs were observed here and from treatment at 200 kHz from PFOS [19]. Although perfluoropropanesulfonic acid (PFPrS) and perfluoropentanesulfonic acid (PFPeS) have been reported from the sonolysis of aqueous film forming foams containing a mix of PFASs [98]. When subject to the same sonolytic conditions as their longer chain counterparts, shorter chain compounds may not degrade with the same efficiency [21], hence a range of possible observations would be made depending on the ultrasonic parameters applied. Cleavage of the terminal ionic functional group was proposed to form a perfluorinated alkyl group, which is easily evaporated into the bubble and mineralised [28]. In the degradation scheme initiated by a hydrated electron, cleavage of the sulfonate group leads to formation of PFOA as observed in this work and at 200 kHz [19], in differing amounts. In sonochemical conditions, PFOA is known to further degrade to shorter chain PFCAs

[19,99]. A combination of the mechanisms (ionic functional group cleavage, sono-intermediate, and/or aqueous electron attack) would also explain the non-stoichiometric release of sulphate reported in some cases and complete mineralisation in others. Hence, hydrated electron-initiated mechanisms could explain the variation in production of shorter chain PFAAs and intermediates and production of PFOA from PFOS observed.

The formation of hydrated electrons at the bubble surface during cavitation has also been reported at high frequency in alkaline conditions [36,119] Eq. (6). However, this step was said to be limited by competition for hydrogen atoms by the comparatively faster reaction of Eq. (7) [35].

$$H + OH^- \leftrightharpoons H_2O + e^-_{aq} \quad (6)$$

$$H + H \rightarrow H_2 \quad (7)$$

Further, no hydrated electrons were detected in bulk solution under argon at 50 kHz [37]. This may be due to the use of a lower frequency and/or the short-lived nature of the electron. In this case Cd^{2+} was used as a scavenger to prevent the reaction of aqueous electrons with spin trap agent α-(4-pyridyl-1-oxide)-*N*-tert butylnitrone (POBN) which can scavenge electrons but not H atoms. However, the cadmium cation would not as readily move to the bubble surface as the spin trap agent POBN, nor would it populate the interface as would be the case for PFOS. Other authors have suggested that solvated electrons allow formation of Cl^- from chloroacetate solutions involving cleavage of the Cl-C bond [38]. This bond energy is significantly lower (~315–330 kcal mol^{-1}) [100] than the C-F bond of PFOS (~440–530 kJ mol^{-1}) [100–102].

In sonolysis, the proposition of the hydrated electron may be countered since, in the presence of 10 mM sodium nitrate, a well-known scavenger of hydrated electrons, the sonolytic degradation rates of 100 μM PFOS and PFOA were not affected [103]. However when sodium nitrate was used as a scavenger, the suppression of PFOA degradation was around 35% in a gas discharge plasma, compared to the almost total suppression of PFOA degradation in a liquid discharge plasma [39]. The means of degradation in the gas discharge plasma were attributed to either high energy electrons or ionised argon in addition to the hydrated electron. In sonolysis and the gas discharge plasma, the degradation of PFOS and many plasma-reactions occur at the gas liquid interface, rather than in the bulk solution, hence the PFOS population could preferentially react with electrons produced.

The main challenge in determining the effects of hydrated electrons is understanding their characteristics at liquid interfaces which have only been elucidated more recently [104,105]. The penetration of electrons into solution was previously said to be limited by their high reactivity and short lifetimes. However, using sensitive optical techniques for short lived species at a plasma liquid interface, the penetration depth before reaction has been measured at (2.5 ± 1.0) nm with an approximate electron concentration of 1 mM at the interface region [104]. Solvated electrons lifetimes at liquid interfaces (such as at the surface of a bubble) were previously calculated to be around 10 ps [106], much lower than in bulk solution [107]. However, more recent studies have shown that lifetimes can be significantly extended to over 100 ps [105]. These new observations suggest that electron activity at the surface of the bubbles may play more of a role in the degradation of surface-active solutes such as PFOS than previously thought.

This also implies that the surface properties of the cavitation bubbles can determine electron lifetimes. The bubble wall can be considered as a concentration shell that constricts on expansion and expands on contraction [84]. Therefore, if the shell is less constricted, it is likely that there will be fewer electron reactions and that they may penetrate farther. Also, if there is deviation from sphericity (increased transience) then this will influence the electrons via changes in the bubble wall properties in which they reside. This, combined with the propensity of PFOS molecules to move to the surface region, may account for the disparity between observance and non-observance of hydrated electron activity, yet the ability for PFOS degradation to occur via electrons in sonolytic conditions.

Therefore, in summary, plasma formation in cavitation bubbles may allow for hydrated electron activity at the surface of the bubbles. These electrons can have longer lifetimes at bubble surfaces, in comparison to bulk solution, and this is also the region where PFOS molecules will tend to reside. Evidence of PFOS degradation via hydrated electrons has been observed using plasmas and electro- and photo-chemical methods. The results of this work have shown that the intensity of collapse, which would support a pyrolytic mechanism, does not readily influence the amount of degradation taking place. Rather, the PFOS degradation was more closely linked with sonochemical effects. Hence, we have proposed that PFOS degradation at the bubble surface may be attributed to chemically-mediated reductive defluorination via the hydrated electron.

3.4. Implications for industrial scale PFOS remediation

Sonolysis has been proven to completely degrade a range of PFASs and PFAS solutions [19,103,108,109] and may be a valuable treatment in environmental PFAS remediation. However, sonolysis is an energy intensive treatment and work must be done to keep efficiency as high as possible. Bulk temperatures will, to some extent, control the dissolved gas concentration which would be higher at lower temperatures and might enhance degradation rates. However, variations in bulk solution temperatures did not appear to play a significant role in enhancing PFAS reaction rates in this work or others [61,63–65]. Therefore, control of bulk temperatures during PFAS sonolysis should be carefully balanced to optimise treatment times against cooling costs, whilst also maintaining temperatures which maintain the lifetime of the ultrasonic devices.

The cost of sonolysis must also be justified against the cost of other possible treatments. A plethora of PFAS treatments exist [7,10,12,13,17,18,110], which can broadly be divided into two categories; removal and destructive technologies. While most removal technologies can be highly efficient for several PFASs, including PFOS, relatively few technologies have been shown to effectively degrade PFOS. A comparison of the efficiency of PFOS degradation processes is shown in Table 4. Works are listed in order of their increasing efficiency, which is based on the G-value method as given previously [20,111]. The G-value was calculated using Eq. (6) below, on a mass basis. Note here that the power was based on the total power drawn for each work (as opposed to calorimetric power) in order to accurately reflect overall treatment efficiency.

$$G_{Value} = \frac{V \bullet (C_{PFAS,0} - C_{PFAS,t})}{P \bullet t} \quad (g\ kWh^{-1}) \quad (6)$$

where;

$V = Treatment\ Volume\,(L)$

$C_{PFAS,t} = PFAS\ concentration\ at\ the\ end\ of\ the\ reaction\,(g\ L^{-1})$

$C_{PFAS,0} = PFAS\ concentration\ at\ the\ start\ of\ the\ reaction\ (g\ L^{-1})$

$P = Drawn\ power\ input\ into\ the\ reactor\ (kW)$

$t = Reaction\ time\ (h)$

Photochemical degradation appears to be slow and inefficient, with significant formation of shorter chains which mitigates treatment (Table 4). This is perhaps due to conversion losses, i.e., during light transmission through the water and conversion of light energy to chemical splitting, due to the ready absorption of electrons generated in the bulk liquid by hydroxyl radicals [117]. The efficiency of sonolysis varies, although this work is one of the more efficient examples, with increased efficiency at higher concentrations [22]. The highest reaction

Table 4
Comparison table of PFOS degradation works and efficiencies.

Technology (Reaction time)	Initial Concentration (mg L^{-1})	Efficiency (g $kW^{-1}h^{-1}$)	Short chain formation	Ref
Photochemical (240 h)	20.0	0.00133	Observed, significant quantity indicated (71% F^- release)	[112]
Photochemical, ferric ion (60 h)	10.0	0.00290	~14% of initial mass	[113]
Sonication, 618 kHz (3 h)	5.00	0.00801	Almost none implied (~100% F^- release)	[28]
Photochemical, persulfate (2 h)	10.0	0.00900	Observed, significant quantity indicated (76% F^- release)	[114]
Photochemical, propanol (24 h)	20.0	0.0152	Not discussed	[112]
Sonication, 400 kHz (4 h)	9.42	0.0155	1% of initial mass	This work
Plasma (4 h)	50.0	0.0260	Not discussed, none implied	[115]
Sonication, 400 kHz (2 h)	9.42	0.0261	13% of initial mass	This work
Sonication, 358 kHz (3 h)	59.5	0.0417	Not discussed	[22]
Plasma (0.5 h)	0.0001	0.0690	Observed, 5.65% of initial mass after 40 min	[39]
Plasma (1 h)	100	0.621	Observed, significant quantity indicated (~30% F^- release)	[116]

rate and efficiency in this work were achieved during the zero-order regime of the reaction (the initial 2 h). This is well explained by saturation of the bubble surface during the zero-order regime, which allows PFOS molecules to readily partition to the bubble surface [19,22]. Hence, cost effectiveness of treatments could be improved with a flow-through system to maintain high PFAS concentrations in the reactor.

Plasma is generally the most efficient and may be because both the photochemical and sonochemical procedures reviewed here were applied in a continuous manner, whereas plasma was applied in pulses. Therefore, the use of pulsed ultrasound may be able to improve the efficiency of sonolysis for PFASs and make it competitive with plasma treatments, since it is known to enhance efficiency in other sonochemical reactions [118]. However, the scalability of plasma [12] and formation of shorter chains (low fluoride release) [111] remain significant challanges, perhaps indicating a selectivity for longer chains and less efficient *complete* mineralisation compared to sonolysis. All the aforementioned technologies are suspected to form aqueous plasma or electrons during PFOS degradation, and no other PFOS degradation mechanisms are known. Hence, PFOS might *only* be degradable via the mechanism proposed of emitted electrons due to the high strength of the C-S bond. Therefore, the most efficient technology might be one which most efficiently generates aqueous plasmas/electrons, which would explain why pulsed plasma generation appears to be the most efficient mode of degradation.

4. Conclusions

In this study, PFOS degradation occurred in the descending order 400 > 500 > 1000 kHz where 96.9, 93.8 and 91.2% degradations were achieved with rates of (1.3 ± 0.49), (1.3 ± 0.03) and (1.0 ± 0.03) × 10^{-2} min^{-1} for 400, 500, and 1000 kHz, respectively. There was also an associated increase in fluoride release, consistent with total mineralisation after 4 h. The close correlation with I_3^- production and SCL intensity suggests conditions which favour radical production also augment PFOS degradation. At 44 kHz, the relative changes in the three processes differed and there was no degradation where SL, SCL, and I_3^- production were present. Under conditions where bubble size was reduced (1000 kHz) and the intensity of collapse did not facilitate a strong SL signal, degradation was able to remain of the same order as the more intense collapse systems. This disparity between the intensity of collapse, bubble surface temperatures (which may not be high enough for pyrolytic degradation of PFOS), knowledge of other hydrated electron PFOS degradation processes and new insights into hydrated electron characteristics led to the conclusion that some degradation is likely taking place via hydrated electrons. It was suggested that conflicting literature on whether hydrated electrons can contribute to degradation of PFOS may be due to the different bubble surface dynamics for different ultrasonic systems and the surface properties of the degradation molecules. Thus, further work is suggested to understand the relationship between these dynamics and the propensity of hydrated electrons to contribute to PFAS / pollutant degradation processes. These findings, and their comparison with those of other technologies, have implications for the future treatment of PFAS pollution as they suggest both bulk liquid and intra-bubble collapse temperatures are less important to PFAS degradation than previously thought and that efficient plasma/aqueous electron generation are critical to cost effective treatment.

CRediT authorship contribution statement

Richard James Wood: Conceptualization, Data curation, Formal analysis, Investigation, Methodology, Project administration, Validation, Writing - original draft, Writing - review & editing. **Tim Sidnell:** Conceptualization, Data curation, Formal analysis, Investigation, Methodology, Project administration, Validation, Writing - original draft, Writing - review & editing. **Ian Ross:** Conceptualization, Funding acquisition, Methodology, Project administration, Supervision, Writing - review & editing. **Jeffrey McDonough:** Writing - review & editing. **Judy Lee:** Conceptualization, Supervision, Writing - review & editing. **Madeleine J. Bussemaker:** Conceptualization, Funding acquisition, Investigation, Methodology, Project administration, Resources, Supervision, Validation, Writing - original draft, Writing - review & editing.

Declaration of Competing Interest

The authors declare that they have no known competing financial interests or personal relationships that could have appeared to influence the work reported in this paper.

Acknowledgements

The authors acknowledge the help and assistance of technical staff within the Department of Chemical and Process Engineering at the University of Surrey, namely, Mr. Chris Burt and Mr. Ben Gibbons, throughout the entirety of this work. This work was partially supported and funded by Arcadis, United Kingdom, Royal Society Research Grant 86200452 and Royal Academy of Engineering Industrial Fellowships Scheme - IFS1819\34

Appendix A. Supplementary data

Supplementary data to this article can be found online at https://doi.org/10.1016/j.ultsonch.2020.105196.

References

[1] J.P. Giesy, K. Kannan, Global distribution of perfluorooctane sulfonate in wildlife, Environ. Sci. Technol. 35 (7) (2001) 1339–1342, https://doi.org/10.1021/es001834k.
[2] R.C. Buck, J. Franklin, U. Berger, et al., Perfluoroalkyl and polyfluoroalkyl substances in the environment: terminology, classification, and origins, Integr. Environ. Assess. Manage. 7 (4) (2011) 513–541, https://doi.org/10.1002/ieam.

258.
[3] I. Ross, E. Kalve, J. McDonough, J. Hurst, J. Miles, T. Pancras, Emerging Contaminants Handbook, Emerging Contaminants Handbook, CRC Press, Boca Raton FL, 2018, pp. 85–257.
[4] E.F. Houtz, D.L. Sedlak, Oxidative conversion as a means of detecting precursors to perfluoroalkyl acids in urban runoff, Environ. Sci. Technol. 46 (17) (2012) 9342–9349, https://doi.org/10.1021/es302274g.
[5] E.F. Houtz, C.P. Higgins, J.A. Field, D.L. Sedlak, Persistence of perfluoroalkyl acid precursors in AFFF-impacted groundwater and soil, Environ. Sci. Technol. 47 (15) (2013) 8187–8195, https://doi.org/10.1021/es4018877.
[6] J.W. Martin, B.J. Asher, S. Beesoon, J.P. Benskin, M.S. Ross, PFOS or PreFOS? Are perfluorooctane sulfonate precursors (PreFOS) important determinants of human and environmental perfluorooctane sulfonate (PFOS) exposure? J. Environ. Monit. 12 (11) (2010) 1979–2004, https://doi.org/10.1039/c0em00295j.
[7] N. Merino, Y. Qu, R.A. Deeb, E.L. Hawley, M.R. Hoffmann, S. Mahendra, Degradation and removal methods for perfluoroalkyl and polyfluoroalkyl substances in water, Environ. Eng. Sci. 33 (9) (2016) 615–649, https://doi.org/10.1089/ees.2016.0233.
[8] J.W.N. Smith, B. Beuthe, M. Dunk, et al., Environmental fate and effects of polyand perfluoroalkyl substances (PFAS), CONCAWE Rep. 8 (2016) 1–107.
[9] P.B. Larsen, E. Giovalle. Perfluoroalkylated Substances: PFOA, PFOS and PFOSA. The Danish Environmental Protection Agency; 2015. http://www2.mst.dk/Udgiv/publications/2015/04/978-87-93283-01-5.pdf.
[10] I. Ross, J. McDonough, J. Miles, et al., A review of emerging technologies for remediation of PFASs, Remediation 28 (2) (2018) 101–126, https://doi.org/10.1002/rem.21553.
[11] E.M. Sunderland, X.C. Hu, C. Dassuncao, A.K. Tokranov, C.C. Wagner, J.G. Allen, A review of the pathways of human exposure to poly- and perfluoroalkyl substances (PFASs) and present understanding of health effects, J. Expo. Sci. Environ. Epidemiol. 29 (2) (2019) 131–147, https://doi.org/10.1038/s41370-018-0094-1.
[12] J. Horst, J. McDonough, I. Ross, et al., Water treatment technologies for PFAS: the next generation, Groundw. Monit. Remediat. 38 (2) (2018) 13–23, https://doi.org/10.1111/gwmr.12281.
[13] C.D. Vecitis, H. Park, J. Cheng, B.T. Mader, M.R. Hoffmann, Treatment technologies for aqueous perfluorooctanesulfonate (PFOS) and perfluorooctanoate (PFOA), Front. Environ. Sci. Eng. China 3 (2) (2009) 129–151, https://doi.org/10.1007/s11783-009-0022-7.
[14] B.E. Smart. Characteristics of CF systems. In: Organofluorine Chemistry. ; 1994:57-88.
[15] M.J. Bentel, Y. Yu, L. Xu, et al., Defluorination of Per- and Polyfluoroalkyl Substances (PFASs) with hydrated electrons: structural dependence and implications to PFAS remediation and management, Environ. Sci. Technol. (2019), https://doi.org/10.1021/acs.est.8b06648.
[16] P. Kirsch, Modern Fluoroorganic Chemistry, Synthesis, Reactivity, Applications, Wiley-VCH, Weinheim, 2004.
[17] V.A. Arias Espana, M. Mallavarapu, R. Naidu, Treatment technologies for aqueous perfluorooctanesulfonate (PFOS) and perfluorooctanoate (PFOA): a critical review with an emphasis on field testing, Environ. Technol. Innov. 4 (2015) 168–181, https://doi.org/10.1016/j.eti.2015.06.001.
[18] K.H. Kucharzyk, R. Darlington, M. Benotti, R. Deeb, E. Hawley, Novel treatment technologies for PFAS compounds: a critical review, J. Environ. Manage. 204 (2017) 757–764, https://doi.org/10.1016/j.jenvman.2017.08.016.
[19] H. Moriwaki, Y. Takagi, M. Tanaka, K. Tsuruho, K. Okitsu, Y. Maeda, Sonochemical decomposition of perfluorooctane sulfonate and perfluorooctanoic acid, Environ. Sci. Technol. 39 (9) (2005) 3388–3392, https://doi.org/10.1021/es040342v.
[20] T. Campbell, M.R. Hoffmann, Sonochemical degradation of perfluorinated surfactants: power and multiple frequency effects, Sep. Purif. Technol. 156 (April) (2015) 1019–1027, https://doi.org/10.1016/j.seppur.2015.09.053.
[21] T.Y. Campbell, C.D. Vecitis, B.T. Mader, M.R. Hoffmann, Perfluorinated surfactant chain-length effects on sonochemical kinetics, J. Phys. Chem. A 113 (36) (2009) 9834–9842, https://doi.org/10.1021/jp903003w.
[22] C.D. Vecitis, H. Park, J. Cheng, B.T. Mader, M.R. Hoffmann, Enhancement of perfluorooctanoate and perfluorooctanesulfonate activity at acoustic cavitation bubble interfaces, J. Phys. Chem. C 112 (43) (2008) 16850–16857, https://doi.org/10.1021/jp804050p.
[23] J. Cheng, C.D. Vecitis, H. Park, B.T. Mader, M.R. Hoffmann, Sonochemical degradation of perfluorooctane sulfonate (PFOS) and perfluorooctanoate (PFOA) in landfill groundwater: environmental matrix effects, Environ. Sci. Technol. 42 (21) (2008) 8057–8063, https://doi.org/10.1021/es8013858.
[24] N.A. Fernandez, L. Rodriguez-Freire, M. Keswani, R. Sierra-Alvarez, Effect of chemical structure on the sonochemical degradation of perfluoroalkyl and polyfluoroalkyl substances (PFASs), Environ. Sci. Water Res. Technol. 2 (6) (2016) 975–983, https://doi.org/10.1039/c6ew00150e.
[25] L. Rodriguez-Freire, R. Balachandran, R. Sierra-Alvarez, M. Keswani, Effect of sound frequency and initial concentration on the sonochemical degradation of perfluorooctane sulfonate (PFOS), J. Hazard. Mater. 300 (2015) 662–669, https://doi.org/10.1016/j.jhazmat.2015.07.077.
[26] V.L. Gole, A. Fishgold, R. Sierra-Alvarez, P. Deymier, M. Keswani, Treatment of perfluorooctane sulfonic acid (PFOS) using a large-scale sonochemical reactor, Sep. Purif. Technol. 2018 (194) (2017) 104–110, https://doi.org/10.1016/j.seppur.2017.11.009.
[27] T. Shende, G. Andaluri, R.P.S. Suri, Kinetic model for sonolytic degradation of non-volatile surfactants: perfluoroalkyl substances, Ultrason. Sonochem. 51 (March) (2019) 359–368, https://doi.org/10.1016/j.ultsonch.2018.08.028.
[28] C.D. Vecitis, H. Park, J. Cheng, B.T. Mader, M.R. Hoffmann, Kinetics and mechanism of the sonolytic conversion of the aqueous perfluorinated surfactants, perfiuorooctanoate (PFOA), and perfluorooctane sulfonate (PFOS) into inorganic products, J. Phys. Chem. A 112 (18) (2008) 4261–4270, https://doi.org/10.1021/jp801081y.
[29] J.A. Gladysz, P. Dennis, T. Horva. Handbook of Fluorous Chemistry.; 2004.
[30] K. Shinoda, M. Hatö, T. Hayashi, The physicochemical properties of aqueous solutions of fluorinated surfactants, J. Phys. Chem. 76 (6) (1972) 909–914, https://doi.org/10.1021/j100650a021.
[31] P. Kanthale, M. Ashokkumar, F. Grieser, Sonoluminescence, sonochemistry (H2O2 yield) and bubble dynamics: Frequency and power effects, Ultrason. Sonochem. 15 (2) (2008) 143–150, https://doi.org/10.1016/j.ultsonch.2007.03.003.
[32] S. Merouani, H. Ferkous, O. Hamdaoui, Y. Rezgui, M. Guemini, A method for predicting the number of active bubbles in sonochemical reactors, Ultrason. Sonochem. 22 (2015) 51–58, https://doi.org/10.1016/j.ultsonch.2014.07.015.
[33] C. Fischer, E. Hart, A. Henglein, Ultrasonic Irradiation of water in the presence of 18,18O2: isotope Exchange and Isotopic Distribution of H2O2, J. Phys. Chem. 5 (1986) 1954–1956.
[34] S.I. Nikitenko, L. Venault, P. Moisy, Scavenging of OH radicals produced from H2O sonolysis with nitrate ions, Ultrason. Sonochem. 11 (2004) 139–142, https://doi.org/10.1063/1.445708.
[35] M. Gutierrez, A. Henglein, J.K. Dohrmann, Hydrogen atom reactions in the sonolysis of aqueous solutions, J. Phys. Chem. 91 (27) (2005) 6687–6690, https://doi.org/10.1021/j100311a026.
[36] G. Cravotto, P. Cintas, Power ultrasound in organic synthesis: Moving cavitational chemistry from academia to innovative and large-scale applications, Chem. Soc. Rev. 35 (2) (2006) 180–196, https://doi.org/10.1039/b503848k.
[37] V. Mišík, P. Riesz, Effect of Cd 2+ on the • H Atom Yield in the Sonolysis of Water. Evidence against the Formation of Hydrated Electrons, J. Phys. Chem. A 101 (8) (2002) 1441–1444, https://doi.org/10.1021/jp963342t.
[38] N.A. Margulis, Mal'tsev, The generation of hydrated electrons in an ultrasonic field, RussJPhysChem. 42 (1968) 1412–1414.
[39] G.R. Stratton, F. Dai, C.L. Bellona, T.M. Holsen, E.R.V. Dickenson, Thagard S. Mededovic, Plasma-based water treatment: efficient transformation of perfluoroalkyl substances in prepared solutions and contaminated groundwater, Environ. Sci. Technol. 51 (3) (2017) 1643–1648, https://doi.org/10.1021/acs.est.6b04215.
[40] Z. Song, H. Tang, N. Wang, L. Zhu, Reductive defluorination of perfluorooctanoic acid by hydrated electrons in a sulfite-mediated UV photochemical system, J. Hazard. Mater. 262 (2013) 332–338, https://doi.org/10.1016/j.jhazmat.2013.08.059.
[41] L. Jin, P. Zhang, Photochemical decomposition of perfluorooctane sulfonate (PFOS) in an anoxic alkaline solution by 185nm vacuum ultraviolet, Chem. Eng. J. 280 (2015) 241–247, https://doi.org/10.1016/j.cej.2015.06.022.
[42] B. Gomez-Ruiz, S. Gómez-Lavín, N. Diban, et al., Efficient electrochemical degradation of poly- and perfluoroalkyl substances (PFASs) from the effluents of an industrial wastewater treatment plant, Chem. Eng. J. 322 (2017) 196–204, https://doi.org/10.1016/j.cej.2017.04.040.
[43] R.J. Wood, J. Lee, M.J. Bussemaker, Disparities between sonoluminescence, sonochemiluminescence and dosimetry with frequency variation under flow, Ultrason. Sonochem. 58 (February) (2019) 104645, , https://doi.org/10.1016/j.ultsonch.2019.104645.
[44] R.J. Wood, J. Lee, M.J. Bussemaker, Combined effects of flow, surface stabilisation and salt concentration in aqueous solution to control and enhance sonoluminescence, Ultrason. Sonochem. 58 (July) (2019) 104683, , https://doi.org/10.1016/j.ultsonch.2019.104683.
[45] R.J. Wood, C. Vévert, J. Lee, M.J. Bussemaker. Flow effects on phenol degradation and sonoluminescence at different ultrasonic frequencies. Ultrason Sonochem. 2020;63(November 2019). DOI:10.1016/j.ultsonch.2019.104892.
[46] R. Pflieger, T. Chave, G. Vite, L. Jouve, S.I. Nikitenko, Effect of operational conditions on sonoluminescence and kinetics of H2O2 formation during the sonolysis of water in the presence of Ar/O2 gas mixture, Ultrason. Sonochem. 26 (2015) 169–175, https://doi.org/10.1016/j.ultsonch.2015.02.005.
[47] R.J. Wood, J. Lee, M.J. Bussemaker, A parametric review of sonochemistry: control and augmentation of sonochemical activity in aqueous solutions, Ultrason. Sonochem. 38 (2017) 351–370, https://doi.org/10.1016/j.ultsonch.2017.03.030.
[48] S. Koda, T. Kimura, T. Kondo, H. Mitome, A standard method to calibrate sonochemical efficiency of an individual reaction system, Ultrason. Sonochem. 10 (3) (2003) 149–156.
[49] R. Pflieger, S.I. Nikitenko, C. Cairós, R. Mettin. Characterization of Cavitation Bubbles and Sonoluminescence. (Springer, ed.). Springer; 2019. DOI:10.1007/978-3-030-11717-7.
[50] T. Ouerhani, R. Pflieger, W. Ben Messaoud, S.I. Nikitenko, Spectroscopy of sonoluminescence and sonochemistry in water saturated with N2-Ar mixtures, J. Phys. Chem. B 119 (52) (2015) 15885–15891, https://doi.org/10.1021/acs.jpcb.5b10221.
[51] C.A. Abeledo, I.M. Kolthoff, The reaction between nitrite and iodide and its application to the iodimetric titration of these anions, J. Am. Chem. Soc. 53 (8) (1931) 2893–2897, https://doi.org/10.1021/ja01359a008.
[52] Hatanaka S. ichi, H. Mitome, K. Yasui, S. Hayashi, Single-bubble sonochemiluminescence in aqueous luminol solutions, J. Am. Chem. Soc. 124 (35) (2002) 10250–10251, https://doi.org/10.1021/ja0258475.
[53] H. McMurray, B. Wilson, Mechanistic and spatial study of ultrasonically induced luminol chemiluminescence, J. Phys. Chem. A 103 (1999) 3955–3962.
[54] J.W. Martin, K. Kannan, U. Berger, et al., Analytical Challenges Hamper, Perfluoroalkyl Res. (2004).
[55] Environmental A. The Determination of Per- and Polyfluorinated Substances

(PFAS) in Water Samples by LC-MS/MS. The Determination of Per- and Polyfluorinated Substances (PFAS) in Water Samples by LC-MS / MS .; 2018.
[56] A. Environmental. Determination of Fluoride by Kone.; 2012. DOI:10.1039/AN9507500510.
[57] A. Environmental. Determination of Anions in Aqueous Matrices Using the Kone Spectrophotometric Analysers, 2017.
[58] T.J. Mason, A.J. Cobley, J.E. Graves, D. Morgan, New evidence for the inverse dependence of mechanical and chemical effects on the frequency of ultrasound, Ultrason. Sonochem. 18 (1) (2011) 226–230, https://doi.org/10.1016/j.ultsonch.2010.05.008.
[59] K.V.B. Tran, T. Kimura, T. Kondo, S. Koda, Quantification of frequency dependence of mechanical effects induced by ultrasound, Ultrason. Sonochem. 21 (2) (2014) 716–721, https://doi.org/10.1016/j.ultsonch.2013.08.018.
[60] A. Brotchie, F. Grieser, M. Ashokkumar, Effect of power and frequency on bubble-size distributions in acoustic cavitation, Phys. Rev. Lett. 102 (8) (2009) 1–4, https://doi.org/10.1103/PhysRevLett.102.084302.
[61] D. Panda, V. Sethu, S. Manickam, Kinetics and mechanism of low-frequency ultrasound driven elimination of trace level aqueous perfluorooctanesulfonic acid and perfluorooctanoic acid, Chem. Eng. Process - Process Intensif. 142 (2019) 107542, , https://doi.org/10.1016/j.cep.2019.107542.
[62] M.Y. Khan, S. So, G. da Silva. Decomposition kinetics of perfluorinated sulfonic acids. Chemosphere. 2020;238. DOI:10.1016/j.chemosphere.2019.124615.
[63] J.C. Lin, S.L. Lo, C.Y. Hu, Y.C. Lee, J. Kuo, Enhanced sonochemical degradation of perfluorooctanoic acid by sulfate ions, Ultrason. Sonochem. 22 (2015) 542–547, https://doi.org/10.1016/j.ultsonch.2014.06.006.
[64] Y.C. Lee, S.L. Lo, J. Kuo, Y.L. Lin, Persulfate oxidation of perfluorooctanoic acid under the temperatures of 20–40°C, Chem. Eng. J. 198–199 (2012) 27–32, https://doi.org/10.1016/j.cej.2012.05.073.
[65] T.A. Bruton, D.L. Sedlak, Treatment of aqueous film-forming foam by heat-activated persulfate under conditions representative of in situ chemical oxidation, Environ. Sci. Technol. 51 (23) (2017) 13878–13885, https://doi.org/10.1021/acs.est.7b03969.
[66] A. Kotronarou, G. Mills, M.R. Hoffmann, Ultrasonic irradiation of p-nitrophenol in aqueous solution, J. Phys. Chem. 95 (9) (1991) 3630–3638, https://doi.org/10.1021/j100162a037.
[67] J.I.E. Cheng, C.D. Vecitis, H. Park, B.T. Mader, A.M.R. Hoffmann, Sonochemical Degradation of Perfluorooctane Sulfonate (PFOS) and Perfluorooctanoate (PFOA) in Groundwater: kinetic effects of matrix inorganics, Environ. Sci. Technol. 44 (1) (2010) 445–450, https://doi.org/10.1021/es8013858.
[68] Y.C. Lee, M.J. Chen, C.P. Huang, J. Kuo, S.L. Lo, Efficient sonochemical degradation of perfluorooctanoic acid using periodate, Ultrason. Sonochem. 31 (2016) 499–505, https://doi.org/10.1016/j.ultsonch.2016.01.030.
[69] A. Brotchie, T. Statham, M. Zhou, L. Dharmarathne, F. Grieser, M. Ashokkumar, Acoustic bubble sizes, coalescence, and sonochemical activity in aqueous electrolyte solutions saturated with different gases, Langmuir 26 (15) (2010) 12690–12695, https://doi.org/10.1021/la1017104.
[70] M.A. Beckett, I. Hua, Impact of ultrasonic frequency on aqueous sonoluminescence and sonochemistry, J. Phys. Chem. A 105 (15) (2001) 3796–3802, https://doi.org/10.1021/jp003226x.
[71] L.A. Crum, G.T. Reynolds, Sonoluminescence produced by "'stable"' cavitation, J. Acoust. Soc. Am. 78 (1) (1985) 137–139, https://doi.org/10.1121/1.392577.
[72] A.A. Ndiaye, R. Pflieger, B. Siboulet, J. Molina, J.F. Dufrêche, S.I. Nikitenko, Nonequilibrium vibrational excitation of OH radicals generated during multi-bubble cavitation in water, J. Phys. Chem. A 116 (20) (2012) 4860–4867, https://doi.org/10.1021/jp301989b.
[73] L.A. Phan Thi, H.T. Do, S.L. Lo, Enhancing decomposition rate of perfluorooctanoic acid by carbonate radical assisted sonochemical treatment, Ultrason. Sonochem. 21 (5) (2014) 1875–1880, https://doi.org/10.1016/j.ultsonch.2014.03.027.
[74] M.A. Beckett, I. Hua, Impact of ultrasonic frequency on aqueous sonoluminescence and sonochemistry, J. Phys. Chem. A 105 (15) (2001) 3796–3802, https://doi.org/10.1021/jp003226x.
[75] T.J. Mason, J.P. Lorimer, Applied Sonochemisty: The Uses of Power Ultrasound in Chemistry and Processing, Wiley, 2002.
[76] M. Ashokkumar, J. Lee, Y. Iida, et al., The detection and control of stable and transient acoustic cavitation bubbles, PCCP 11 (43) (2009) 10118–10121, https://doi.org/10.1039/b915715h.
[77] E. Ciawi, J. Rae, M. Ashokkumar, F. Grieser, Determination of temperatures within acoustically generated bubbles in aqueous solutions at different ultrasound frequencies, J. Phys. Chem. B 110 (27) (2006) 13656–13660, https://doi.org/10.1021/jp061441t.
[78] M. Ashokkumar, J. Lee, Y. Iida, et al., Spatial distribution of acoustic cavitation bubbles at different ultrasound frequencies, ChemPhysChem 11 (8) (2010) 1680–1684, https://doi.org/10.1002/cphc.200901037.
[79] K. Yasui, T. Tuziuti, T. Kozuka, A. Towata, Y. Iida, Relationship between the bubble temperature and main oxidant created inside an air bubble under ultrasound, J. Chem. Phys. 127 (15) (2007), https://doi.org/10.1063/1.2790420.
[80] G.J. Price, M. Ashokkumar, F. Grieser, Sonoluminescence quenching of organic compounds in aqueous solution: frequency effects and implications for sonochemistry, J. Am. Chem. Soc. 126 (9) (2004) 2755–2762, https://doi.org/10.1021/ja0389624.
[81] M. Ashokkumar, R. Hall, P. Mulvaney, F. Grieser, Sonoluminescence from aqueous alcohol and surfactant solutions, J. Phys. Chem. B 101 (50) (2002) 10845–10850, https://doi.org/10.1021/jp972477b.
[82] J. Lee, S.E. Kentish, M. Ashokkumar, The effect of surface-active solutes on bubble coalescence in the presence of ultrasound, J. Phys. Chem. B 109 (11) (2005) 5095–5099, https://doi.org/10.1021/jp0476444.
[83] J. Lee, I.U. Vakarelski, K. Yasiui, et al., Variations in the spatial distribution of sonoluminescing bubbles in the presence of an ionic surfactant and electrolyte, J. Phys. Chem. B 114 (8) (2010) 2572–2577, https://doi.org/10.1021/jp907329z.
[84] L.A. Crum, Acoustic cavitation series: part five rectified diffusion, Ultrasonics 22 (5) (1984) 215–223, https://doi.org/10.1016/0041-624X(84)90016-7.
[85] T. Leong, J. Collis, R. Manasseh, et al., The role of surfactant headgroup, chain length, and cavitation microstreaming on the growth of bubbles by rectified diffusion, J. Phys. Chem. C 115 (49) (2011) 24310–24316, https://doi.org/10.1021/jp208862p.
[86] M.P. Brenner, S. Hilgenfeldt, D. Lohse, Single-bubble sonoluminescence, Rev. Mod. Phys. 74 (2002) 425–484.
[87] W.B. McNamara, Y.T. Didenko, K.S. Suslick, Sonoluminescence temperatures during multi-bubble cavitation, Nature 401 (6755) (1999) 772–775, https://doi.org/10.1038/44536.
[88] M. Ashokkumar, K. Vinodgopal, F. Grieser, Sonoluminescence quenching in aqueous solutions containing weak organic acids and bases and its relevance to sonochemistry, J. Phys. Chem. B 104 (27) (2000) 6447–6451, https://doi.org/10.1021/jp9937407.
[89] H. Xu, N.C. Eddingsaas, K.S. Suslick, Spatial separation of cavitating bubble populations: the nanodroplet injection model, J. Am. Chem. Soc. 131 (17) (2009) 6060–6061, https://doi.org/10.1021/ja900457v.
[90] T. Yamada, P.H. Taylor. Final Report - Lab Scale Thermal Degradation of PFOS and Related Precursors, 2003.
[91] T. Yamada, P.H. Taylor, R.C. Buck, M.A. Kaiser, R.J. Giraud, Thermal degradation of fluorotelomer treated articles and related materials, Chemosphere 61 (7) (2005) 974–984, https://doi.org/10.1016/j.chemosphere.2005.03.025.
[92] M.M. Schultz, D.F. Barofsky, J.A. Field, Fluorinated Alkyl Surfactants, Env. Eng. Sci. 20 (5) (2003) 487–501.
[93] P.H. Taylor, T. Yamada, R.C. Striebich, J.L. Graham, R.J. Giraud, Investigation of waste incineration of fluorotelomer-based polymers as a potential source of PFOA in the environment, Chemosphere 110 (2014) 17–22, https://doi.org/10.1016/j.chemosphere.2014.02.037.
[94] K.S. Suslick, D.A. Hammerton, R.E. Cline, The Sonochemical Hot Spot, J. Am. Chem. Soc. 108 (18) (1986) 5641–5642, https://doi.org/10.1021/ja00278a055.
[95] S.I. Nikitenko, R. Pflieger, Toward a new paradigm for sonochemistry: short review on nonequilibrium plasma observations by means of MBSL spectroscopy in aqueous solutions, Ultrason. Sonochem. 35 (2017) 623–630, https://doi.org/10.1016/j.ultsonch.2016.02.003.
[96] S. Khalid, B. Kappus, K. Weninger, S. Putterman, Opacity and transport measurements reveal that dilute plasma models of sonoluminescence are not valid, Phys. Rev. Lett. 108 (10) (2012) 1–5, https://doi.org/10.1103/PhysRevLett.108.104302.
[97] V. Kamath, A. Prosperetti, F.N. Egolfopoulos, A theoretical study of sonoluminescence, J. Acoust. Soc. Am. 94 (1) (2005) 248–260, https://doi.org/10.1121/1.407083.
[98] L. Rodriguez-Freire, N. Abad-Fernández, R. Sierra-Alvarez, et al., Sonochemical degradation of perfluorinated chemicals in aqueous film-forming foams, J. Hazard. Mater. 317 (2016) 275–283, https://doi.org/10.1016/j.jhazmat.2016.05.078.
[99] S.C. Panchangam, A.Y.C. Lin, J.H. Tsai, C.F. Lin, Sonication-assisted photocatalytic decomposition of perfluorooctanoic acid, Chemosphere 75 (5) (2009) 654–660, https://doi.org/10.1016/j.chemosphere.2008.12.065.
[100] G. Glockler, Carbon-halogen bond energies and bond distances, J. Phys. Chem. 63 (6) (1959) 828–832, https://doi.org/10.1021/j150576a013.
[101] 3M. The Science of Organic Fluorochemistry. 1999:1-12. http://www.fluoridealert.org/wp-content/pesticides/pfos.fr.final.docket.0006.pdf.
[102] D. O'Hagan, Understanding organofluorine chemistry. An introduction to the C-F bond, Chem. Soc. Rev. 37 (2) (2008) 308–319, https://doi.org/10.1039/b711844a.
[103] J. Cheng, C.D. Vecitis, H. Park, B.T. Mader, M.R. Hoffmann, Sonochemical degradation of perfluorooctane sulfonate (PFOS) and perfluorooctanoate (PFOA) in groundwater: kinetic effects of matrix inorganics, Environ. Sci. Technol. 44 (1) (2010) 445–450, https://doi.org/10.1021/es902651g.
[104] P. Rumbach, D.M. Bartels, R.M. Sankaran, D.B. Go, The solvation of electrons by an atmospheric-pressure plasma, Nat. Commun. (2015) 6, https://doi.org/10.1038/ncomms8248.
[105] K.R. Siefermann, Y. Liu, E. Lugovoy, et al., Binding energies, lifetimes and implications of bulk and interface solvated electrons in water, Nat. Chem. 2 (4) (2010) 274–279, https://doi.org/10.1038/nchem.580.
[106] Á. Madarász, P.J.J. Rossky, L. Turi, Excess electron relaxation dynamics at water/air interfaces, J. Chem. Phys. 126 (23) (2007), https://doi.org/10.1063/1.2741514.
[107] K. Yokoyama, C. Silva, D.H. Son, P.K. Walhout, P.F. Barbara, Detailed investigation of the femtosecond pump-probe spectroscopy of the hydrated electron, J. Phys. Chem. A 102 (35) (1998) 6957–6966, https://doi.org/10.1021/jp981809p.
[108] T.Y. Campbell, C.D. Vecitis, B.T. Mader, M.R. Hoffmann, Perfluorinated surfactant chain-length effects on sonochemical kinetics, J. Phys. Chem. A 113 (36) (2009) 9834–9842, https://doi.org/10.1021/jp903003w.
[109] V.L. Gole, A. Fishgold, R. Sierra-Alvarez, P. Deymier, M. Keswani, Treatment of perfluorooctane sulfonic acid (PFOS) using a large-scale sonochemical reactor, Sep. Purif. Technol. 194 (November 2017) (2018) 104–110, https://doi.org/10.1016/j.seppur.2017.11.009.
[110] D. Banks, B. Jun, J. Heo, N. Her, C. Min, Selected advanced water treatment technologies for perfluoroalkyl and polyfluoroalkyl substances: a review, Sep. Purif. Technol. 231 (August 2019) (2020), https://doi.org/10.1016/j.seppur.2019.115929 115929.

[111] J.C. Lin, C.Y. Hu, S.L. Lo, Effect of surfactants on the degradation of perfluorooctanoic acid (PFOA) by ultrasonic (US) treatment, Ultrason. Sonochem. 28 (2016) 130–135, https://doi.org/10.1016/j.ultsonch.2015.07.007.
[112] T. Yamamoto, Y. Noma, S.I. Sakai, Y. Shibata, Photodegradation of perfluorooctane sulfonate by UV irradiation in water and alkaline 2-propanol, Environ. Sci. Technol. 41 (16) (2007) 5660–5665, https://doi.org/10.1021/es0706504.
[113] L. Jin, P. Zhang, T. Shao, S. Zhao, Ferric ion mediated photodecomposition of aqueous perfluorooctane sulfonate (PFOS) under UV irradiation and its mechanism, J. Hazard. Mater. 271 (2014) 9–15, https://doi.org/10.1016/j.jhazmat.2014.01.061.
[114] H. Park, C.D. Vecitis, J. Cheng, N.F. Dalleska, B.T. Mader, M.R. Hoffmann, Reductive degradation of perfluoroalkyl compounds with aquated electrons generated from iodide photolysis at 254 nm, Photochem. Photobiol. Sci. 10 (12) (2011) 1945–1953, https://doi.org/10.1039/c1 pp05270e.
[115] K. Yasuoka, K. Sasaki, R. Hayashi, An energy-efficient process for decomposing perfluorooctanoic and perfluorooctane sulfonic acids using dc plasmas generated within gas bubbles, Plasma Sources Sci. Technol. 20 (3) (2011), https://doi.org/10.1088/0963-0252/20/3/034009.
[116] A.J. Lewis, T. Joyce, M. Hadaya et al. Rapid degradation of PFAS in aqueous solutions by reverse vortex flow gliding arc plasma. 2020. DOI:10.1039/c9ew01050e.
[117] I. Sirés, E. Brillas, Remediation of water pollution caused by pharmaceutical residues based on electrochemical separation and degradation technologies: a review, Environ. Int. 40 (1) (2012) 212–229, https://doi.org/10.1016/j.envint.2011.07.012.
[118] T. Tuziuti, K. Yasui, J. Lee, T. Kozuka, A. Towata, Y. Iida, Mechanism of enhancement of sonochemical-reaction efficiency by pulsed ultrasound, J. Phys. Chem. A 112 (22) (2008) 4875–4878, https://doi.org/10.1021/jp802640x.
[119] Dharmarathne Leena, Muthupandian Ashokkumar, Franz Grieser, On the generation of the hydrated electron during the sonolysis of aqueous solutions, J. Phys. Chem. A 117 (12) (2013) 2409–2414, https://doi.org/10.1021/jp312389n.